Layer-multiple-scattering method for photonic crystals of nonspherical particles

G. Gantzounis and N. Stefanou
Section of Solid State Physics, University of Athens, Panepistimioupolis, GR-157 84 Athens, Greece
(Received 2 November 2005; revised manuscript received 2 December 2005; published 10 January 2006)

We present an extension of the layer-multiple-scattering method to photonic crystals of nonspherical particles in a homogeneous host medium. The efficiency of the method is demonstrated on a specific example of a crystal of metallic spheroids. We report a thorough analysis of the optical properties of this crystal and discuss aspects of the underlying physics that relate to the nonspherical shape of the particles.

DOI: 10.1103/PhysRevB.73.035115 PACS number(s): 42.70.Qs, 42.25.Bs, 73.20.Mf, 78.67.Bf

I. INTRODUCTION

The layer-multiple-scattering method (LMSM) is very efficient for the evaluation of the optical properties of three-dimensional (3D) photonic crystals consisting of nonoverlapping spherical scatterers in a homogeneous host medium.[1–6] An important aspect of the method is that, contrary to traditional band-structure or time-domain methods, it proceeds at a given frequency, i.e., it is an "on-shell" method. Therefore, it can be directly applied to photonic crystals made of strongly dispersive building components such as real metals,[7–13] ionic materials in the infrared region,[14,15] doped semiconductors,[14] etc., thus exploring the impressive opportunities offered by the resonant behavior of the permittivity and/or permeability of these materials in different regions of frequency. Moreover, because of the on-shell character of the method, absorption and/or gain in the constituent materials can be treated in a straightforward manner. Besides the complex frequency band structure of an infinite photonic crystal, associated with a given crystallographic plane, the LMSM allows one to calculate, also, the transmission, reflection and absorption coefficients of an electromagnetic (EM) wave incident at a given angle on a finite slab of the crystal and, therefore, it can describe an actual transmission experiment. An advantage of the method is that it does not require periodicity in the direction perpendicular to the layers: the layers must only have the same two-dimensional (2D) periodicity. Therefore a number of interesting applications, such as planar defects, heterostructures, and photonic crystal slabs on homogeneous plates and substrates, can be also treated in a more or less straightforward manner.[16–22] Finally, the LMSM can incorporate multiple-scattering Green's-function techniques[23–26] that allow one to calculate the (local) density of states of the EM field, as well as to treat defects and disorder. This enables one to study a variety of interesting physical phenomena, including waveguiding and Anderson localization.

The LMSM has been proven very efficient for photonic crystals of spherical particles, such as colloidal crystals, opals, systems of microspheres, etc.[27–31] With the same efficiency, it can treat, also, spherical particles consisting of an arbitrary number of concentric spherical shells by a powerful recursive algorithm.[32,33] Moreover, the method can be, in principle, extended to systems of nonspherical particles, because the scattering properties of the individual particles enter only through the corresponding T matrix. However, in this case, the convergence of the method must be carefully examined and its efficiency needs to be demonstrated.

In this paper, we report an extension of LMSM to photonic crystals of nonspherical particles. We use the extended-boundary-condition method (EBCM) for the evaluation of the scattering T matrix of the individual particles[34] and demonstrate the efficiency of the method on a specific example of a photonic crystal of metallic spheroidal particles. We analyze transmission and absorption spectra of finite slabs of this crystal in conjunction with relevant complex-band-structure and density-of-states diagrams, demonstrating the physical origin of the field eigenmodes as well as the differences from corresponding systems of spherical particles. Potential applications of photonic crystals of nonspherical particles are also anticipated.

II. SCATTERING BY A NONSPHERICAL PARTICLE

The electric field associated with a harmonic, monochromatic EM wave, of angular frequency ω, has the form $\mathbf{E}(\mathbf{r},t)=\mathrm{Re}[\mathbf{E}(\mathbf{r})\exp(-i\omega t)]$. For a plane wave of wave vector $\mathbf{q}$, propagating in a homogeneous medium characterized by a relative dielectric function ϵ and a relative magnetic permeability μ (we shall denote it by an index 0), we have

$$\mathbf{E}_0(\mathbf{r}) = \hat{\mathbf{p}} E_0(\mathbf{q}) \exp(i\mathbf{q}\cdot\mathbf{r}), \tag{1}$$

where E_0 is the magnitude and $\hat{\mathbf{p}}$, a unit vector, the polarization of the electric field. The plane wave given by Eq. (1) can be expanded into regular vector spherical waves about a given origin of coordinates as follows:[2,3]

$$\mathbf{E}_0(\mathbf{r}) = \sum_{\ell=1}^{\infty} \sum_{m=-\ell}^{\ell} \left(\frac{i}{q} a^0_{E\ell m} \boldsymbol{\nabla} \times j_\ell(qr) \mathbf{X}_{\ell m}(\hat{\mathbf{r}}) + a^0_{H\ell m} j_\ell(qr) \mathbf{X}_{\ell m}(\hat{\mathbf{r}}) \right), \tag{2}$$

where $q=\omega\sqrt{\epsilon\mu}/c$, c being the velocity of light in vacuum; $j_\ell(qr)$ are the spherical Bessel functions which are finite everywhere; and $\mathbf{X}_{\ell m}(\hat{\mathbf{r}})$ are the vector spherical harmonics. The coefficients $a^0_{P\ell m}$, $P=E,H$, can be written as

$$a^0_{P\ell m} = \mathbf{A}^0_{P\ell m}(\mathbf{q}) \cdot \hat{\mathbf{p}} E_0(\mathbf{q}), \tag{3}$$

with

$$\mathbf{A}^0_{E\ell m}(\mathbf{q}) = \frac{4\pi i^\ell (-1)^{m+1}}{\sqrt{\ell(\ell+1)}} \times \{ i[\alpha^m_\ell e^{i\phi} Y_{\ell,-m-1}(\hat{\mathbf{q}}) - \alpha^{-m}_\ell e^{-i\phi} Y_{\ell,-m+1}(\hat{\mathbf{q}})]\hat{\mathbf{e}}_1 - [\alpha^m_\ell \cos\theta\, e^{i\phi} Y_{\ell,-m-1}(\hat{\mathbf{q}}) + m \sin\theta Y_{\ell,-m}(\hat{\mathbf{q}}) + \alpha^{-m}_\ell \cos\theta\, e^{-i\phi} Y_{\ell,-m+1}(\hat{\mathbf{q}})]\hat{\mathbf{e}}_2 \} \quad (4)$$

and

$$\mathbf{A}^0_{H\ell m}(\mathbf{q}) = \frac{4\pi i^\ell (-1)^{m+1}}{\sqrt{\ell(\ell+1)}} \{ [\alpha^m_\ell \cos\theta\, e^{i\phi} Y_{\ell,-m-1}(\hat{\mathbf{q}}) + m \sin\theta Y_{\ell,-m}(\hat{\mathbf{q}}) + \alpha^{-m}_\ell \cos\theta\, e^{-i\phi} Y_{\ell,-m+1}(\hat{\mathbf{q}})]\hat{\mathbf{e}}_1 + i[\alpha^m_\ell e^{i\phi} Y_{\ell,-m-1}(\hat{\mathbf{q}}) - \alpha^{-m}_\ell e^{-i\phi} Y_{\ell,-m+1}(\hat{\mathbf{q}})]\hat{\mathbf{e}}_2 \}, \quad (5)$$

where $\alpha^m_\ell \equiv \frac{1}{2}[(\ell-m)(\ell+m+1)]^{1/2}$; $(\theta,\phi) \equiv \hat{\mathbf{q}}$ denote the angular variables of $\mathbf{q}$ in the chosen system of spherical coordinates; and $\hat{\mathbf{e}}_1, \hat{\mathbf{e}}_2$ are the polar and azimuthal unit vectors, respectively, which are perpendicular to $\mathbf{q}$.

We now consider a homogeneous particle of arbitrary shape, centered at the origin of coordinates, and assume that its relative dielectric function ϵ_s and/or magnetic permeability μ_s, in general complex functions of ω, are different from those of the surrounding medium. When the plane wave described by Eq. (2) is incident on the particle, it is scattered by it, so that the wave field outside the particle consists of the incident wave and a scattered wave, which can be expanded in spherical waves as follows:

$$\mathbf{E}_{\mathrm{sc}}(\mathbf{r}) = \sum_{\ell m} \left(\frac{i}{q} a^+_{E\ell m} \boldsymbol{\nabla} \times h^+_\ell(qr)\mathbf{X}_{\ell m}(\hat{\mathbf{r}}) + a^+_{H\ell m} h^+_\ell(qr)\mathbf{X}_{\ell m}(\hat{\mathbf{r}}) \right), \quad (6)$$

where $h^+_\ell(qr)$ are the spherical Hankel functions appropriate to outgoing spherical waves: $h^+_\ell(qr) \approx (-i)^\ell \exp(iqr)/iqr$ as $r \to \infty$. On the other hand, the wave field inside the particle, which must be finite at the origin, has the form

$$\mathbf{E}_{\mathrm{I}}(\mathbf{r}) = \sum_{\ell m} \left(\frac{i}{q_s} a^{\mathrm{I}}_{E\ell m} \boldsymbol{\nabla} \times j_\ell(q_s r)\mathbf{X}_{\ell m}(\hat{\mathbf{r}}) + a^{\mathrm{I}}_{H\ell m} j_\ell(q_s r)\mathbf{X}_{\ell m}(\hat{\mathbf{r}}) \right), \quad (7)$$

where $q_s = \sqrt{\epsilon_s \mu_s}\,\omega/c$.

In general the coefficients $a^+_{P\ell m}$ of the scattered wave can be expressed in terms of those of the incident wave ($a^0_{P\ell m}$) through the scattering T matrix as follows:

$$a^+_{P\ell m} = \sum_{P'\ell'm'} T_{P\ell m;P'\ell'm'} a^0_{P'\ell'm'}. \quad (8)$$

Among the methods suggested for the calculation of the T matrix, EBCM appears to be very efficient. This method takes into account the boundary condition of continuity of the tangential components of the EM field on the surface of the scatterer through appropriate surface integrals.[34] This leads to linear equations of the form

$$a^0_{P\ell m} = \sum_{P'\ell'm'} Q^0_{P\ell m;P'\ell'm'} a^{\mathrm{I}}_{P'\ell'm'} \quad (9)$$

and

$$a^+_{P\ell m} = \sum_{P'\ell'm'} Q^+_{P\ell m;P'\ell'm'} a^{\mathrm{I}}_{P'\ell'm'} \quad (10)$$

which, substituted into Eq. (8), give

$$\sum_{P''\ell''m''} T_{P\ell m;P''\ell''m''} Q^+_{P''\ell''m'';P'\ell'm'} = -Q^0_{P\ell m;P'\ell'm'}. \quad (11)$$

The matrix elements of $\mathbf{Q}^0$ and $\mathbf{Q}^+$ are given in terms of integrals of simple expressions involving spherical Bessel and Hankel functions over the surface of the scatterer.

Although the spherical-wave expansions of the EM field are infinite series, it turns out that, if the size of the particle is not much larger than the wavelength, a limited number of partial waves, corresponding to $\ell \leqslant \ell_{\max}$, is sufficient for the description of the scattered field and of the T matrix. However, in order to accurately solve Eq. (11), we must keep matrix elements up to ℓ_{cut} ($\geqslant \ell_{\max}$). The fact that ℓ_{cut} significantly increases as the shape of the particle deviates from the sphere means that, in order to accurately evaluate the elements of the T matrix of given dimensions, a large number of Q-matrix elements are needed. Obviously, for spherical particles we have $\ell_{\mathrm{cut}} = \ell_{\max}$. We note that Eq. (11) should not be solved through inversion of $\mathbf{Q}^+$, because this procedure may induce numerical instabilities; it should be considered as a linear system of equations and solved, e.g., by Gaussian elimination with an overflow control.[35]

In the case of axially symmetric particles which have a mirror plane normal to the symmetry axis, such as spheroids, cylinders, etc., one obtains the following simple formulas for the matrix elements of $\mathbf{Q}^+$ and $\mathbf{Q}^0$

$$Q^{+(0)}_{E\ell m;E\ell'm'} = q^2 J^{+(0)}_{E\ell m;H\ell'm'} - qq_s \frac{\mu}{\mu_s} J^{+(0)}_{H\ell m;E\ell'm'},$$

$$Q^{+(0)}_{H\ell m;H\ell'm'} = qq_s \frac{\mu}{\mu_s} J^{+(0)}_{E\ell m;H\ell'm'} - q^2 J^{+(0)}_{H\ell m;E\ell'm'},$$

$$Q^{+(0)}_{E\ell m;H\ell'm'} = qq_s \frac{\mu}{\mu_s} J^{+(0)}_{E\ell m;E\ell'm'} + q^2 J^{+(0)}_{H\ell m;H\ell'm'},$$

$$Q^{+(0)}_{H\ell m;E\ell'm'} = -q^2 J^{+(0)}_{E\ell m;E\ell'm'} - qq_s \frac{\mu}{\mu_s} J^{+(0)}_{H\ell m;H\ell'm'}, \quad (12)$$

where

$$J^{+}_{E\ell m;H\ell' m'} = \frac{2\pi i \delta_{mm'}[1+(-1)^{\ell+\ell'}]}{\sqrt{\ell(\ell+1)\ell'(\ell'+1)}} \int_0^1 d(\cos\theta) r^2 h^{+}_{\ell}(qr) \Bigg[\frac{1}{q_s r}\frac{\partial}{\partial r}[r j_{\ell'}(q_s r)] \Bigg(\frac{m^2}{\sin^2\theta} Y_{\ell' m}(\theta) Y_{\ell m}(\theta) + \frac{\partial Y_{\ell' m}(\theta)}{\partial\theta}\frac{\partial Y_{\ell m}(\theta)}{\partial\theta} \Bigg)$$
$$+ \ell'(\ell'+1)\frac{\partial \ln r}{\partial\theta}\frac{j_{\ell'}(q_s r)}{q_s r} Y_{\ell' m}(\theta)\frac{\partial Y_{\ell m}(\theta)}{\partial\theta} \Bigg],$$

$$J^{+}_{H\ell m;E\ell' m'} = \frac{2\pi i \delta_{mm'}[1+(-1)^{\ell+\ell'}]}{\sqrt{\ell(\ell+1)\ell'(\ell'+1)}} \int_0^1 d(\cos\theta) r^2 j_{\ell'}(q_s r) \Bigg[\frac{1}{qr}\frac{\partial}{\partial r}[r h^{+}_{\ell}(qr)] \Bigg(\frac{m^2}{\sin^2\theta} Y_{\ell' m}(\theta) Y_{\ell m}(\theta) + \frac{\partial Y_{\ell' m}(\theta)}{\partial\theta}\frac{\partial Y_{\ell m}(\theta)}{\partial\theta} \Bigg)$$
$$+ \ell(\ell+1)\frac{\partial \ln r}{\partial\theta}\frac{h^{+}_{\ell}(qr)}{qr} Y_{\ell m}(\theta)\frac{\partial Y_{\ell' m}(\theta)}{\partial\theta} \Bigg],$$

$$J^{+}_{E\ell m;E\ell' m'} = \frac{2\pi i \delta_{mm'}[1-(-1)^{\ell+\ell'}]}{\sqrt{\ell(\ell+1)\ell'(\ell'+1)}} \int_0^1 d(\cos\theta) \frac{m r^2}{\sin\theta} \Bigg[\frac{1}{qr}\frac{\partial}{\partial r}[r h^{+}_{\ell}(qr)] \frac{1}{q_s r}\frac{\partial}{\partial r}[r j_{\ell'}(q_s r)] \Bigg(Y_{\ell m}(\theta)\frac{\partial Y_{\ell' m}(\theta)}{\partial\theta} + Y_{\ell' m}(\theta)\frac{\partial Y_{\ell m}(\theta)}{\partial\theta} \Bigg)$$
$$+ \frac{\partial \ln r}{\partial\theta} \Bigg(\ell'(\ell'+1)\frac{j_{\ell'}(q_s r)}{q_s r}\frac{1}{qr}\frac{\partial}{\partial r}[r h^{+}_{\ell}(qr)] + \ell(\ell+1)\frac{h^{+}_{\ell}(qr)}{qr}\frac{1}{q_s r}\frac{\partial}{\partial r}[r j_{\ell'}(q_s r)] \Bigg) Y_{\ell m}(\theta) Y_{\ell' m}(\theta) \Bigg],$$

$$J^{+}_{H\ell m;H\ell' m'} = \frac{2\pi i \delta_{mm'}[1-(-1)^{\ell+\ell'}]}{\sqrt{\ell(\ell+1)\ell'(\ell'+1)}} \int_0^1 d(\cos\theta) \frac{m r^2}{\sin\theta} h^{+}_{\ell}(qr) j_{\ell'}(q_s r) \Bigg(Y_{\ell m}(\theta)\frac{\partial Y_{\ell' m}(\theta)}{\partial\theta} + Y_{\ell' m}(\theta)\frac{\partial Y_{\ell m}(\theta)}{\partial\theta} \Bigg), \tag{13}$$

and $J^{0}_{P\ell m;P'\ell' m'}$ are given by the same expressions as $J^{+}_{P\ell m;P'\ell' m'}$ with $j_\ell(qr)$ in the place of $h^{+}_{\ell}(qr)$. In Eqs. (13), $Y_{\ell m}(\theta)$ denotes the spherical harmonic $Y_{\ell m}(\theta,\phi=0)$, and $r \equiv r(\theta)$ is the distance of a given point on the surface of the particle from the origin.

The factor $\delta_{mm'}$ in Eqs. (13) implies that Eqs. (11) split into independent systems of equations, one system for each value of m. Moreover, because of the factor $[1\pm(-1)^{\ell+\ell'}]$ in Eqs. (13), the matrix elements of $\mathbf{Q}^{+}$ and $\mathbf{Q}^{0}$ for PP': EH,HE or EE,HH vanish identically if $\ell+\ell'$ is an even or an odd integer, respectively, according to Eqs. (12). Therefore, each of the above-mentioned systems of equations can be further reduced into two independent subsystems. We also note that one need not calculate $Q^{+(0)}_{P\ell m;P'\ell' m'}$ for negative values of m because, according to Eqs. (12) and (13), $Q^{+(0)}_{P\ell -m;P'\ell' -m} = (2\delta_{PP'}-1) Q^{+(0)}_{P\ell m;P'\ell' m}$.

With the help of the T matrix, defined above, one can calculate directly the change in the number of states up to a frequency ω between the system under consideration (a single scatterer in a host medium) and that of the host medium extending over all space as follows:

$$\Delta N(\omega) = \frac{1}{\pi}\,\mathrm{Im}\ln\det(\mathbf{I}+\mathbf{T}), \tag{14}$$

where $\mathbf{I}$ is the unit matrix.[23,25] Of more interest is the difference in the density of states induced by the scatterer, given by $\Delta n(\omega) = d\Delta N(\omega)/d\omega$. The scattering and extinction cross section can be also obtained from the T matrix through the equations

$$\sigma_{\mathrm{sc}} = \frac{1}{q^2}\sum_{P\ell m}\Bigg| \sum_{P'\ell' m'} T_{P\ell m;P'\ell' m'} \mathbf{A}^{0}_{P'\ell' m'}\cdot\hat{\mathbf{p}} \Bigg|^2$$

$$\sigma_{\mathrm{ext}} = -\frac{1}{q^2}\,\mathrm{Re}\sum_{P\ell m}(\mathbf{A}^{0}_{P\ell m}\cdot\hat{\mathbf{p}})^{*} \sum_{P'\ell' m'} T_{P\ell m;P'\ell' m'} \mathbf{A}^{0}_{P'\ell' m'}\cdot\hat{\mathbf{p}}, \tag{15}$$

while the absorption cross section is $\sigma_{\mathrm{abs}} = \sigma_{\mathrm{ext}} - \sigma_{\mathrm{sc}}$. It is clear that, except for the case of spheres, the cross sections depend on the polarization and the direction of propagation of the incident wave.

In the present work we shall consider metallic particles characterized by $\mu_s = 1$ and a Drude relative dielectric function[36]

$$\epsilon_s(\omega) = 1 - \frac{\omega_p^2}{\omega(\omega + i\tau^{-1})}, \tag{16}$$

where ω_{p} is the bulk plasma frequency and τ the relaxation time of the conduction-band electrons of the metal, in air ($\epsilon=1$, $\mu=1$). We assume, to begin with, a single oblate spheroid with major axis $A = 2.065c/\omega_p$ and minor axis $B = 1.877c/\omega_p$, the latter being the axis of revolution z, and compare it to a sphere of equal volume with radius $S = c/\omega_p$. For the numerical calculations we use $\ell_{\max}=4$, $\ell_{\mathrm{cut}}=6$, and a Gaussian quadrature integration formula with ten points for the integrals in Eqs. (13). The results obtained have a relative error less than 10^{-5}.

The eigenmodes of the EM field, i.e., solutions of Eq. (8) in the absence of an incident wave, are obtained at the poles of the T matrix. In the case of a metallic sphere

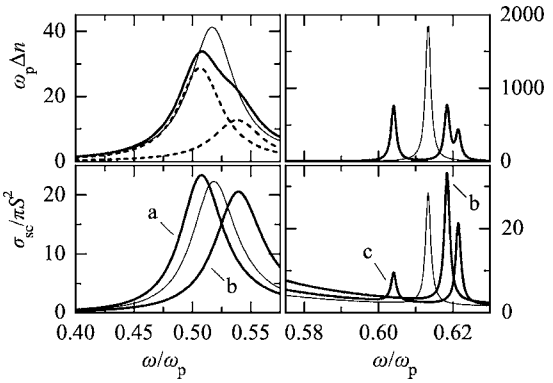

FIG. 1. Left panel: The change in the density of states (upper diagram) induced by a nonabsorbing metallic oblate spheroid ($A=2.065c/\omega_p$, $B=1.877c/\omega_p$) in air, about the dipole resonances. The corresponding scattering cross section is shown in the lower diagram for incidence along the z direction (a), and along the x direction with polarization along the z axis (b). Right panel: The change in the density of states (upper diagram) about the quadrupole resonances. The corresponding scattering cross section is shown in the lower diagram for incidence along the x direction with polarization along the z axis (b), and for incidence at an angle 45° with respect to the z axis with polarization in the xz plane (c). The thin lines in all the diagrams show the corresponding results for a sphere of equal volume ($S=c/\omega_p$).

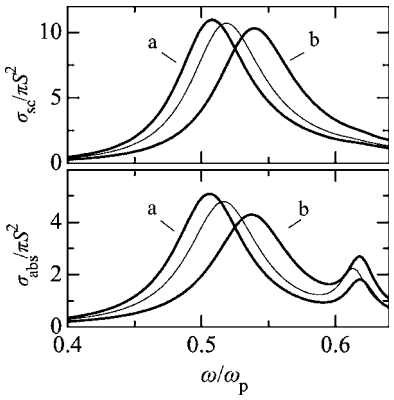

FIG. 2. The scattering (upper diagram) and the absorption (lower diagram) cross sections of a metallic oblate spheroid ($A=2.065c/\omega_p$, $B=1.877c/\omega_p$) for incidence along the z direction (a), and along the x direction with polarization along the z axis (b). The thin lines in the diagrams show the corresponding results for a sphere of equal volume ($S=c/\omega_p$).

($T_{P\ell m;P'\ell'm'}=T_{P\ell}\delta_{PP'}\delta_{\ell\ell'}\delta_{mm'}$) such poles exist near the real frequency axis for $P=E$. The eigenfrequencies of these so-called surface- or particle-plasmon (because they correspond to 2^ℓ-pole collective electron oscillations at the surface of the particle) modes, in the limit $qS, q_sS \ll 1$, are given by $\omega_\ell \simeq \omega_p\sqrt{\ell/[\ell+(\ell+1)\epsilon]}$,[21] and the degeneracy of each mode is $2\ell+1$. In the case of nonspherical particles there is no clear characterization of multipole modes, since the T matrix is no longer diagonal. However, for nearly spherical particles, one can still characterize the modes as *mainly* dipole, quadrupole, etc.

In the left panel of Fig. 1 we show the change in the density of states and the scattering cross section for the oblate spheroid and the corresponding sphere in air, in the frequency region about the dipole surface-plasmon modes. It can be seen that shape anisotropy induces a mode splitting, an effect which can result, also, from permittivity anisotropy. The threefold degeneracy of the dipole surface-plasmon mode for the sphere is removed in the case of the spheroid, giving rise to two Lorentian peaks in the density of states,[21] shown by the broken curves in the upper left diagram of Fig. 1. The center of each Lorentzian gives the eigenfrequency and its half width at half maximum gives the inverse of the lifetime of the corresponding mode. The low-frequency peak at $0.506\omega_p$ is associated with a twofold degenerate dipole mode (the area of the peak equals 2) which corresponds to surface-plasma oscillations normal to the z axis ($m=\pm 1$), and is excited by an incident wave polarized normal to this axis. The high-frequency peak at $0.538\omega_p$ is associated with a nondegenerate dipole mode (the area of the peak equals unity) which corresponds to surface-plasma oscillations parallel to the z axis ($m=0$), and is excited by an incident wave polarized along this axis. It is worth noting that a sphere with diameter equal to the major axis of the spheroid exhibits a dipole peak at $0.515\omega_p$, whereas for a sphere with diameter equal to the minor axis of the spheroid this peak appears at $0.524\omega_p$, i.e., the shift of the peak position relative to that of the equal-volume sphere (at $0.517\omega_p$) is not as large as that obtained in the case of the spheroid. It should be also noted that the calculated eigenfrequencies of the dipole modes are not very close to the nonretardation result, $\omega_1=\omega_p/\sqrt{3}=0.577\omega_p$, for a spherical particle, because the conditions qS, $q_sS \ll 1$ are not satisfied in the case under consideration. In the right panel of Fig. 1 we show the change in the density of states and the scattering cross section for the spheroid and the corresponding sphere in air, in the frequency region about the quadrupole surface-plasmon modes. This fivefold degenerate mode in the case of the sphere is split in the case of the spheroid into one nondegenerate ($m=0$ at $0.621\omega_p$) and two twofold degenerate ($m=\pm 1$ at $0.618\omega_p$ and $m=\pm 2$ at $0.604\omega_p$) modes. While the excitation of the dipole surface-plasmon modes depends only on the polarization of the incident wave, the excitation of the higher multipole modes depends also on the direction of incidence. For example, a plane EM wave incident along the x axis with a polarization along the z axis excites the $m=\pm 1$ quadrupole mode, while a wave incident at an angle 45° with respect to the z axis and polarization in the xz plane excites both the $m=\pm 2$ and the $m=0$ quadrupole modes, as shown in the lower right diagram of Fig. 1.

In Fig. 2 we show the scattering and absorption cross sections of the particles, if we take into account dissipative losses in the metal assuming $\tau^{-1}=0.025\omega_p$ in Eq. (16), which is a typical value for metals. It can be seen from Fig. 2 that the quadrupole surface-plasmon modes are fully absorbed: they do not manifest themselves in the scattering cross section and appear as small and broad peaks in the absorption cross section. This happens because these modes have very long lifetimes, as compared to the relaxation time.

III. A PERIODIC MONOLAYER OF NONSPHERICAL PARTICLES

We consider a plane of nonoverlapping particles, at $z=0$, which are centered on the sites $\mathbf{R}_n$ of a given 2D lattice. Let the plane wave, described by Eq. (1), be incident on this layer. Because of the 2D periodicity of the structure under consideration, we write the component of the wave vector of the incident wave parallel to the layer, $\mathbf{q}_\parallel$, as $\mathbf{q}_\parallel=\mathbf{k}_\parallel+\mathbf{g}'$ where $\mathbf{k}_\parallel$, the reduced wave vector in the surface Brillouin zone (SBZ), is a conserved quantity in the scattering process and $\mathbf{g}'$ is a certain reciprocal vector of the given lattice. Therefore, the wave vector of the incident wave has the form $\mathbf{K}_{\mathbf{g}'}^{\pm}=\mathbf{k}_\parallel+\mathbf{g}'\pm[q^2-(\mathbf{k}_\parallel+\mathbf{g}')^2]^{1/2}\hat{\mathbf{e}}_z$, where $\hat{\mathbf{e}}_z$ is the unit vector along the z axis and the $+$ or $-$ sign refers to incidence from the left ($z<0$) or from the right ($z>0$). The corresponding electric field is written as

$$\mathbf{E}_{\mathrm{in}}^{s'}(\mathbf{r})=[E_{\mathrm{in}}]_{\mathbf{g}'i'}^{s'}\exp(i\mathbf{K}_{\mathbf{g}'}^{s'}\cdot\mathbf{r})\hat{\mathbf{e}}_{i'}, \tag{17}$$

where $s'=+$ or $-$, and $i'=1$ or 2 corresponds to a p- or s-polarized wave, $\hat{\mathbf{e}}_1,\hat{\mathbf{e}}_2$ being the polar and azimuthal unit vectors, respectively, which are perpendicular to $\mathbf{K}_{\mathbf{g}'}^{s'}$. According to Eq. (3), the coefficients $a_{P\ell m}^0$ in the expansion (2) of the plane wave (17) are

$$a_{P\ell m}^0=A_{P\ell m;i'}^0(\mathbf{K}_{\mathbf{g}'}^{s'})[E_{\mathrm{in}}]_{\mathbf{g}'i'}^{s'}\quad\text{for } P=E,H. \tag{18}$$

Because of the 2D periodicity of the array of particles, the wave scattered by it, when the wave (17) is incident upon it, has the following form:

$$\mathbf{E}_{\mathrm{sc}}(\mathbf{r})=\sum_{\mathbf{R}_n}\exp(i\mathbf{k}_\parallel\cdot\mathbf{R}_n)\sum_{\ell m}\left(\frac{i}{q}b_{E\ell m}^{+}\boldsymbol{\nabla}\times h_\ell^{+}(qr_n)\mathbf{X}_{\ell m}(\hat{\mathbf{r}}_n)+b_{H\ell m}^{+}h_\ell^{+}(qr_n)\mathbf{X}_{\ell m}(\hat{\mathbf{r}}_n)\right), \tag{19}$$

where $\mathbf{r}_n=\mathbf{r}-\mathbf{R}_n$. The coefficients $b_{P\ell m}^{+}$, which depend linearly on the amplitude of the incident wave, can be written as follows:

$$b_{P\ell m}^{+}=B_{P\ell m;i'}^{+}(\mathbf{K}_{\mathbf{g}'}^{s'})[E_{\mathrm{in}}]_{\mathbf{g}'i'}^{s'}. \tag{20}$$

We obtain $\mathbf{B}_{P\ell m}^{+}$ in terms of $\mathbf{A}_{P\ell m}^0$ by solving the following system of linear equations:[3]

$$\sum_{P'\ell'm'}\left(\delta_{PP'}\delta_{\ell\ell'}\delta_{mm'}-\sum_{P''\ell''m''}T_{P\ell m;P''\ell''m''}\Omega_{P''\ell''m'';P'\ell'm'}\right)\times B_{P'\ell'm';i'}^{+}(\mathbf{K}_{\mathbf{g}'}^{s'})=\sum_{P'\ell'm'}T_{P\ell m;P'\ell'm'}A_{P'\ell'm';i'}^0(\mathbf{K}_{\mathbf{g}'}^{s'}), \tag{21}$$

where the matrix elements $\Omega_{P\ell m;P'\ell'm'}$ depend on the geometry of the layer, on the reduced wave vector $\mathbf{k}_\parallel$, and on the frequency ω of the incident wave; they depend also on the dielectric function of the medium surrounding the particles, but they do not depend on the scattering properties of the individual particles. Explicit expressions for these matrix elements are given in Ref. 2.

If we assign to the index P the integer values 1 and 2 instead of the symbols E and H, respectively, both the matrix elements $T_{P\ell m;P'\ell'm'}$, as defined for the symmetric particles of Sec. II, and $\Omega_{P\ell m;P'\ell'm'}$ vanish when $P+\ell+m$ and $P'+\ell'+m'$ have not the same parity. Therefore the system of Eqs. (21) can be readily reduced to two subsystems, as follows:

$$\sum_{o'}\left(\delta_{oo'}-\sum_{o''}T_{oo''}\Omega_{o''o'}\right)B_{o'}^{+}(\mathbf{K}_{\mathbf{g}'}^{s'})=\sum_{o'}T_{oo'}A_{o';i'}^0(\mathbf{K}_{\mathbf{g}'}^{s'}),$$

$$\sum_{e'}\left(\delta_{ee'}-\sum_{e''}T_{ee''}\Omega_{e''e'}\right)B_{e'}^{+}(\mathbf{K}_{\mathbf{g}'}^{s'})=\sum_{e'}T_{ee'}A_{e';i'}^0(\mathbf{K}_{\mathbf{g}'}^{s'}), \tag{22}$$

where the $o(e)$ index enumerates the matrix elements that correspond to $P+\ell+m$ odd (even) integer in the sense mentioned above.

Since ω and $\mathbf{k}_\parallel$ are conserved quantities in the scattering process, the scattered field, given by Eq. (19), will consist of a series of plane waves with wave vectors

$$\mathbf{K}_{\mathbf{g}}^{\pm}=\mathbf{k}_\parallel+\mathbf{g}\pm[q^2-(\mathbf{k}_\parallel+\mathbf{g})^2]^{1/2}\hat{\mathbf{e}}_z\quad\forall\,\mathbf{g} \tag{23}$$

and polarizations along $\hat{\mathbf{e}}_1$ and $\hat{\mathbf{e}}_2$ (polar and azimuthal unit vectors, respectively, associated with every $\mathbf{K}_{\mathbf{g}}^{s}$, $s=\pm$). Therefore we write

$$\mathbf{E}_{\mathrm{sc}}^{s}(\mathbf{r})=\sum_{\mathbf{g}}\sum_{i=1}^{2}[E_{\mathrm{sc}}]_{\mathbf{g}i}^{s}\exp(i\mathbf{K}_{\mathbf{g}}^{s}\cdot\mathbf{r})\hat{\mathbf{e}}_i, \tag{24}$$

where the superscript $s=+$ $(-)$ holds for $z>0$ $(z<0)$. Though the scattered wave consists, in general, of a number of diffracted beams corresponding to different 2D reciprocal-lattice vectors $\mathbf{g}$, only beams for which $K_{\mathbf{g}z}^{s}$ is real constitute propagating waves. When $(\mathbf{k}_\parallel+\mathbf{g})^2>q^2$ the corresponding wave decays to the right for $s=+$, and to the left for $s=-$; and the corresponding unit vectors $\hat{\mathbf{e}}_i$ become complex but they are still orthonormal ($\hat{\mathbf{e}}_i\cdot\hat{\mathbf{e}}_j=\delta_{ij}$, $i,j=1,2$). The coefficients in Eq. (24) can be expressed through $b_{P\ell m}^{+}$ as follows:[3]

$$[E_{\mathrm{sc}}]_{\mathbf{g}i}^{s}=\sum_{P\ell m}\Delta_{P\ell m;i}(\mathbf{K}_{\mathbf{g}}^{s})b_{P\ell m}^{+}, \tag{25}$$

with $\boldsymbol{\Delta}_{P\ell m}(\mathbf{K}_{\mathbf{g}}^{s})$ given by

$$\begin{aligned}\boldsymbol{\Delta}_{E\ell m}(\mathbf{K}_{\mathbf{g}}^{s})=&\frac{2\pi(-i)^\ell}{qA_0K_{\mathbf{g}z}^{+}\sqrt{\ell(\ell+1)}}\\&\times\{i[\alpha_\ell^{-m}e^{i\phi}Y_{\ell m-1}(\hat{\mathbf{K}}_{\mathbf{g}}^{s})-\alpha_\ell^{m}e^{-i\phi}Y_{\ell m+1}(\hat{\mathbf{K}}_{\mathbf{g}}^{s})]\hat{\mathbf{e}}_1\\&-[\alpha_\ell^{-m}\cos\theta\,e^{i\phi}Y_{\ell m-1}(\hat{\mathbf{K}}_{\mathbf{g}}^{s})-m\sin\theta\,Y_{\ell m}(\hat{\mathbf{K}}_{\mathbf{g}}^{s})\\&+\alpha_\ell^{m}\cos\theta\,e^{-i\phi}Y_{\ell m+1}(\hat{\mathbf{K}}_{\mathbf{g}}^{s})]\hat{\mathbf{e}}_2\},\end{aligned}$$

$$\mathbf{\Delta}_{H\ell m}(\mathbf{K}_{\mathbf{g}}^{s}) = \frac{2\pi(-i)^{\ell}}{qA_0K_{\mathbf{g}z}^{+}\sqrt{\ell(\ell+1)}}\{[\alpha_{\ell}^{-m}\cos\theta\, e^{i\phi}Y_{\ell m-1}(\hat{\mathbf{K}}_{\mathbf{g}}^{s}) - m\sin\theta\, Y_{\ell m}(\hat{\mathbf{K}}_{\mathbf{g}}^{s}) + \alpha_{\ell}^{m}\cos\theta\, e^{-i\phi}Y_{\ell m+1}(\hat{\mathbf{K}}_{\mathbf{g}}^{s})]\hat{\mathbf{e}}_1 + i[\alpha_{\ell}^{-m}e^{i\phi}Y_{\ell m-1}(\hat{\mathbf{K}}_{\mathbf{g}}^{s}) - \alpha_{\ell}^{m}e^{-i\phi}Y_{\ell m+1}(\hat{\mathbf{K}}_{\mathbf{g}}^{s})]\hat{\mathbf{e}}_2\}, \tag{26}$$

where θ, ϕ denote the angular variables $(\hat{\mathbf{K}}_{\mathbf{g}}^{s})$ of $\mathbf{K}_{\mathbf{g}}^{s}$, and A_0 is the area of the unit cell of the 2D lattice. We note that, according to Eq. (25), $[E_{\mathrm{sc}}]_{\mathbf{g}i}^{s}$ depend on the incident plane wave through the coefficients $B_{P\ell m;i'}^{+}(\mathbf{K}_{\mathbf{g}'}^{s'})$ which are evaluated from Eqs. (22).

For example, when a plane wave (17) is incident on the layer from the left, the transmitted wave (incident + scattered) on the right of the layer is given by

$$\mathbf{E}_{\mathrm{tr}}^{+}(\mathbf{r}) = \sum_{\mathbf{g}i}[E_{\mathrm{tr}}]_{\mathbf{g}i}^{+}\exp(i\mathbf{K}_{\mathbf{g}}^{+}\cdot\mathbf{r})\hat{\mathbf{e}}_i, \quad z>0, \tag{27}$$

with

$$[E_{\mathrm{tr}}]_{\mathbf{g}i}^{+} = [E_{\mathrm{in}}]_{\mathbf{g}'i'}^{+}\delta_{\mathbf{g}\mathbf{g}'}\delta_{ii'} + [E_{\mathrm{sc}}]_{\mathbf{g}i}^{+} = M_{\mathbf{g}i;\mathbf{g}'i'}^{++}[E_{\mathrm{in}}]_{g'i'}^{+}, \tag{28}$$

and the reflected wave on the left of the layer by

$$\mathbf{E}_{\mathrm{rf}}^{-}(\mathbf{r}) = \sum_{\mathbf{g}i}[E_{\mathrm{rf}}]_{\mathbf{g}i}^{-}\exp(i\mathbf{K}_{\mathbf{g}}^{-}\cdot\mathbf{r})\hat{\mathbf{e}}_i, \quad z<0, \tag{29}$$

with

$$[E_{\mathrm{rf}}]_{\mathbf{g}i}^{-} = [E_{\mathrm{sc}}]_{\mathbf{g}i}^{-} = M_{\mathbf{g}i;\mathbf{g}'i'}^{-+}[E_{\mathrm{in}}]_{g'i'}^{+}. \tag{30}$$

Similarly, we can define the transmission matrix elements $M_{\mathbf{g}i;\mathbf{g}'i'}^{--}$ and the reflection matrix elements $M_{\mathbf{g}i;\mathbf{g}'i'}^{+-}$ for a plane wave incident on the layer from the right. Using Eq. (25) we obtain

$$M_{\mathbf{g}i;\mathbf{g}'i'}^{ss'} = \delta_{ss'}\delta_{\mathbf{g}\mathbf{g}'}\delta_{ii'} + \sum_{P\ell m}\Delta_{P\ell m;i}(\mathbf{K}_{\mathbf{g}}^{s})B_{P\ell m;i'}^{+}(\mathbf{K}_{\mathbf{g}'}^{s'}). \tag{31}$$

The matrix elements $M_{\mathbf{g}i;\mathbf{g}'i'}^{ss'}$ obey the symmetry relation $M_{\mathbf{g}i;\mathbf{g}'i'}^{-s-s'} = (-1)^{i+i'}M_{\mathbf{g}i;\mathbf{g}'i'}^{ss'}$.

After calculating the transmitted and reflected waves, when a plane wave (17) is incident on the given layer, we can proceed to the calculation of the transmittance $\mathcal{T}(\omega,\mathbf{k}_{\parallel}+\mathbf{g}',i')$ and the reflectance $\mathcal{R}(\omega,\mathbf{k}_{\parallel}+\mathbf{g}',i')$ of the layer. These are defined as the ratio of the transmitted (reflected) energy flux to the energy flux associated with the incident wave. Assuming, e.g., incidence from the left, we obtain

$$\mathcal{T} = \frac{\sum_{\mathbf{g}i}|[E_{\mathrm{tr}}]_{\mathbf{g}i}^{+}|^2K_{\mathbf{g}z}^{+}}{|[E_{\mathrm{in}}]_{\mathbf{g}'i'}^{+}|^2K_{\mathbf{g}'z}^{+}} \tag{32}$$

and

$$\mathcal{R} = \frac{\sum_{\mathbf{g}i}|[E_{\mathrm{rf}}]_{\mathbf{g}i}^{-}|^2K_{\mathbf{g}z}^{+}}{|[E_{\mathrm{in}}]_{\mathbf{g}'i'}^{+}|^2K_{\mathbf{g}'z}^{+}}. \tag{33}$$

We remember that only propagating beams (those with $K_{\mathbf{g}z}^{+}$ real) enter the numerators of the above equations. Finally we note that if absorption is present it can be calculated from the requirement of energy conservation: $\mathcal{A}=1-\mathcal{T}-\mathcal{R}$.

The difference in the number of states up to a given frequency ω, between the system under consideration (a plane of particles in a homogeneous medium) and that of the host medium extending over all space is given by

$$\Delta N(\omega) = \frac{N}{A}\int\int_{SBZ}d^2k_{\parallel}\Delta N(\omega,\mathbf{k}_{\parallel}), \tag{34}$$

where N is the number of surface unit cells of the plane of particles and A the area of the SBZ. The $\mathbf{k}_{\parallel}$-resolved change in the number of states is given, in the spherical-wave representation, by

$$\Delta N(\omega,\mathbf{k}_{\parallel}) = \frac{1}{\pi}\,\mathrm{Im}\ln\det(\mathbf{I}+\mathbf{T}) - \frac{1}{\pi}\,\mathrm{Im}\ln\det(\mathbf{I}-\mathbf{T}\mathbf{\Omega}), \tag{35}$$

and in the plane-wave representation by

$$\Delta N(\omega,\mathbf{k}_{\parallel}) = \frac{1}{2\pi}\,\mathrm{Im}\ln\det\mathbf{S}, \tag{36}$$

where the S matrix is identical to the M matrix defined by Eqs. (31).[25,26] We note that the S matrix is defined in the basis of those reciprocal-lattice vectors which correspond to propagating beams and that the resulting $\Delta N(\omega,\mathbf{k}_{\parallel})$, contrary to that obtained through Eq. (35), does not include possible bound states of the system. The $\mathbf{k}_{\parallel}$-resolved change in the density of states is obtained through $\Delta n(\omega,\mathbf{k}_{\parallel}) = \partial\Delta N(\omega,\mathbf{k}_{\parallel})/\partial\omega$.

We demonstrate the applicability of the formalism presented in this section on a specific example: a square array, with lattice constant $a=6.5c/\omega_p$, of nonabsorbing metallic oblate spheroids, with $A=2.065c/\omega_p$ and $B=1.877c/\omega_p$, in air. For the given system it is sufficient to truncate the relevant spherical-wave expansions at $\ell_{\max}=4$ and use $\ell_{\mathrm{cut}}=6$ for the calculation of the T matrix (see Sec. II). Figure 3 shows the change in the density of states of the system with respect to air, for $\mathbf{k}_{\parallel}=\mathbf{0}$, and the corresponding transmittance, in the frequency region of the dipole surface-plasmon modes. For $\mathbf{k}_{\parallel}=\mathbf{0}$, the square symmetry of the system implies that the states of the EM field have the symmetry of the irreducible representations of the C_{4v} group: Δ_1, Δ_2, $\Delta_{1'}$, $\Delta_{2'}$, and Δ_5.[37] The states of symmetry Δ_1, Δ_2, $\Delta_{1'}$, and $\Delta_{2'}$ are nondegenerate, and Δ_5 are doubly degenerate. We note that a plane EM wave propagating in the host region normal to the given layer has the Δ_5 symmetry and, therefore, only the doubly degenerate modes of the layer can be excited by an externally incident wave (see lower diagram of Fig. 3). The nondegenerate modes (of Δ_1 symmetry in the present case) are inactive; they are bound states of the system and decay exponentially to zero away from the layer on either side of it.

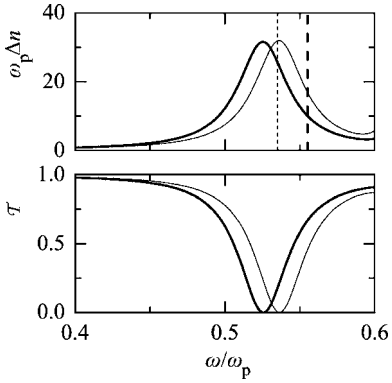

FIG. 3. Change in the density of states (upper diagram) of a square array, with lattice constant $a=6.5c/\omega_p$, of nonabsorbing metallic oblate spheroids ($A=2.065c/\omega_p$, $B=1.877c/\omega_p$), with respect to air, for $\mathbf{k}_\parallel=\mathbf{0}$ (the vertical broken lines show the position of the bound states), and transmittance (lower diagram) at normal incidence. The thin lines in the diagrams show the corresponding results if the spheroids are replaced by spheres of equal volume ($S=c/\omega_p$).

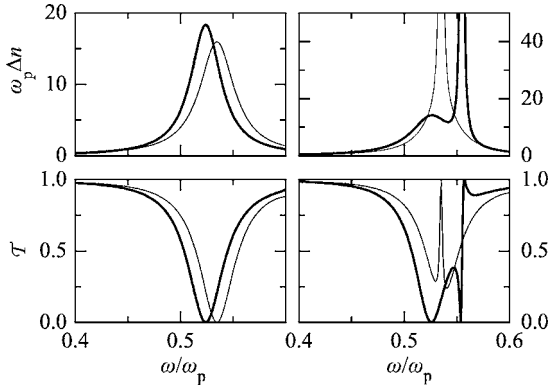

FIG. 4. A square array, with lattice constant $a=6.5c/\omega_p$, of nonabsorbing metallic oblate spheroids ($A=2.065c/\omega_p$, $B=1.877c/\omega_p$), in air. Upper panel: The change in the density of states of Q_2 (left diagram) and Q_1 (right diagram) symmetry of the system, for $\mathbf{k}_\parallel=(0.3\pi/a,0)$, with respect to air. Lower panel: Transmittance of an s- (left diagram) and a p- (right diagram) polarized wave incident on the layer with the same $\mathbf{k}_\parallel$. The thin lines in all the diagrams show the corresponding results if the spheroids are replaced by spheres of equal volume ($S=c/\omega_p$).

These inactive modes are delta functions in the density of states, while the optically active modes, of Δ_5 symmetry, are manifested as Lorentzian peaks in the density of states (see upper diagram of Fig. 3). The integral of each such Lorentzian equals two, while its center and width determine the eigenfrequency and inverse lifetime, respectively, of the corresponding mode. The doubly degenerate dipole mode of the single spheroid gives a Δ_5 resonant state at $0.525\omega_p$, with an inverse lifetime $0.020\omega_p$, while its nondegenerate dipole mode gives a bound state of Δ_1 symmetry at $0.555\omega_p$. It can be seen that the position of the dipole modes of the single spheroid is shifted in the case of the plane of spheroids because of the interaction between them. In the case of the corresponding plane of spheres, the three-fold degenerate dipole mode gives a bound state of symmetry Δ_1 at $0.535\omega_p$ and a Δ_5 resonant state at $0.536\omega_p$, with an inverse lifetime $0.020\omega_p$.

Let us now consider off-normal incidence with $\mathbf{k}_\parallel=(k_x,0)$. In this case the point group of the system is the C_{1h} group. This group has two one-dimensional irreducible representations: Q_1 and Q_2, with basis functions which are even (Q_1) and odd (Q_2) upon reflection with respect to the xz plane. We note that a plane EM wave propagating in the host medium with the given $\mathbf{k}_\parallel$ has the Q_2 or Q_1 symmetry if it is s or p polarized, respectively. A Δ_1 mode in the case of $\mathbf{k}_\parallel=\mathbf{0}$ is now reduced to a mode of Q_1 symmetry which is excited by a p-polarized incident wave, as shown in the right panel of Fig. 4. Similarly, a Δ_5 mode splits into a Q_1 and a Q_2 mode. As can be seen in Fig. 4, these modes manifest themselves as Lorentzian peaks of area equal to unity in the density of states, and as complex resonance structures in the corresponding transmission spectra.[15]

In Fig. 5 we show the transmittance and absorbance of the given layer, if we take into account dissipative losses in the metallic material ($\tau^{-1}=0.025\omega_p$), for $\mathbf{k}_\parallel=(0.3\pi/a,0)$ and p polarization. It can be seen that sharp features in the transmission spectra associated with resonant modes of long lifetime are smoothed out by absorption. This is clearly discerned in the case of the plane of spheroids, where the corresponding broad and narrow resonances are well separated. As a result one obtains a more uniform absorbance over a relatively broad frequency range as compared with the case of spherical particles, a property which may be useful in the way of practical applications.

IV. A PHOTONIC CRYSTAL OF NONSPHERICAL PARTICLES

In order to describe scattering by multilayers of particles with the same 2D periodicity, it is convenient to express the waves on the left of a given layer with respect to an origin $\mathbf{A}_l$ on the left of the layer at $-\mathbf{d}_l$ from its center and the waves

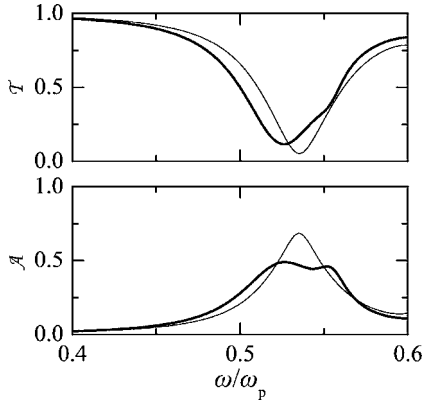

FIG. 5. Transmittance (upper diagram) and absorbance (lower diagram) of a square array, with lattice constant $a=6.5c/\omega_p$, of absorbing metallic oblate spheroids ($A=2.065c/\omega_p$, $B=1.877c/\omega_p$), in air, for $\mathbf{k}_\parallel=(0.3\pi/a,0)$ and p polarization. The thin lines in the diagrams show the corresponding results if the spheroids are replaced by spheres of equal volume ($S=c/\omega_p$).

on the right of this layer with respect to an origin $\mathbf{A}_r$ on the right of the layer at $\mathbf{d}_r$ from its center, i.e., a plane wave on the left of the layer will be written as $\mathbf{E}^s_{\mathbf{g}} \exp[i\mathbf{K}^s_{\mathbf{g}} \cdot (\mathbf{r}-\mathbf{A}_l)]$ and a plane wave on the right of the layer will be written as $\mathbf{E}^s_{\mathbf{g}} \exp[i\mathbf{K}^s_{\mathbf{g}} \cdot (\mathbf{r}-\mathbf{A}_r)]$. With the above choice of origins the transmission (reflection) matrix elements of a layer become

$$Q^{\mathrm{I}}_{\mathbf{g}i;\mathbf{g}'i'} = M^{++}_{\mathbf{g}i;\mathbf{g}'i'} \exp[i(\mathbf{K}^+_{\mathbf{g}} \cdot \mathbf{d}_r + \mathbf{K}^+_{\mathbf{g}'} \cdot \mathbf{d}_l)],$$

$$Q^{\mathrm{II}}_{\mathbf{g}i;\mathbf{g}'i'} = M^{+-}_{\mathbf{g}i;\mathbf{g}'i'} \exp[i(\mathbf{K}^+_{\mathbf{g}} \cdot \mathbf{d}_r - \mathbf{K}^-_{\mathbf{g}'} \cdot \mathbf{d}_r)],$$

$$Q^{\mathrm{III}}_{\mathbf{g}i;\mathbf{g}'i'} = M^{-+}_{\mathbf{g}i;\mathbf{g}'i'} \exp[-i(\mathbf{K}^-_{\mathbf{g}} \cdot \mathbf{d}_l - \mathbf{K}^+_{\mathbf{g}'} \cdot \mathbf{d}_l)],$$

$$Q^{\mathrm{IV}}_{\mathbf{g}i;\mathbf{g}'i'} = M^{--}_{\mathbf{g}i;\mathbf{g}'i'} \exp[-i(\mathbf{K}^-_{\mathbf{g}} \cdot \mathbf{d}_l + \mathbf{K}^-_{\mathbf{g}'} \cdot \mathbf{d}_r)]. \quad (37)$$

The transmission (reflection) matrices for a multilayer slab are obtained from the corresponding matrices of the individual layers, in the manner described in Ref. 2. For a plane wave $[E_{\mathrm{in}}]^+_{\mathbf{g}'i'} \exp[i\mathbf{K}^+_{\mathbf{g}'} \cdot (\mathbf{r}-\mathbf{A}_{\mathrm{L}})]\hat{\mathbf{e}}_{i'}$, incident on the slab from the left, we finally obtain a reflected wave $\Sigma_{\mathbf{g}i}[E_{\mathrm{rf}}]^-_{\mathbf{g}i} \exp[i\mathbf{K}^-_{\mathbf{g}} \cdot (\mathbf{r}-\mathbf{A}_{\mathrm{L}})]\hat{\mathbf{e}}_i$ on the left of the slab and a transmitted wave $\Sigma_{\mathbf{g}i}[E_{\mathrm{tr}}]^+_{\mathbf{g}i} \exp[i\mathbf{K}^+_{\mathbf{g}} \cdot (\mathbf{r}-\mathbf{A}_{\mathrm{R}})]\hat{\mathbf{e}}_i$ on the right of the slab, where $\mathbf{A}_{\mathrm{L}}$ ($\mathbf{A}_{\mathrm{R}}$) is the appropriate origin at the left (right) interface of the slab. We have

$$[E_{\mathrm{tr}}]^+_{\mathbf{g}i} = Q^{\mathrm{I}}_{\mathbf{g}i;\mathbf{g}'i'} [E_{\mathrm{in}}]^+_{\mathbf{g}'i'}, \quad (38)$$

$$[E_{\mathrm{rf}}]^-_{\mathbf{g}i} = Q^{\mathrm{III}}_{\mathbf{g}i;\mathbf{g}'i'} [E_{\mathrm{in}}]^+_{\mathbf{g}'i'}, \quad (39)$$

where $\mathbf{Q}^{\mathrm{I}}$ and $\mathbf{Q}^{\mathrm{III}}$ are the appropriate transmission and reflection matrices of the slab. After calculating the transmitted and reflected waves on the right and left of the slab, we can obtain the corresponding transmittance $\mathcal{T}(\omega, \mathbf{k}_{\parallel}+\mathbf{g}', i')$ and reflectance $\mathcal{R}(\omega, \mathbf{k}_{\parallel}+\mathbf{g}', i')$ from Eqs. (32) and (33), respectively. On the other hand, the change in the number of states between the slab and the homogeneous host medium extending over all space can be calculated from Eqs. (34) and (36), where the elements of the S matrix in the plane-wave representation are given by

$$S^{++}_{\mathbf{g}i;\mathbf{g}'i'} = \exp[-i(\mathbf{K}^+_{\mathbf{g}} \cdot \mathbf{A}_{\mathrm{R}} - \mathbf{K}^+_{\mathbf{g}'} \cdot \mathbf{A}_{\mathrm{L}})] Q^{\mathrm{I}}_{\mathbf{g}i;\mathbf{g}'i'},$$

$$S^{+-}_{\mathbf{g}i;\mathbf{g}'i'} = \exp[-i(\mathbf{K}^+_{\mathbf{g}} \cdot \mathbf{A}_{\mathrm{R}} - \mathbf{K}^-_{\mathbf{g}'} \cdot \mathbf{A}_{\mathrm{R}})] Q^{\mathrm{II}}_{\mathbf{g}i;\mathbf{g}'i'},$$

$$S^{-+}_{\mathbf{g}i;\mathbf{g}'i'} = \exp[-i(\mathbf{K}^-_{\mathbf{g}} \cdot \mathbf{A}_{\mathrm{L}} - \mathbf{K}^+_{\mathbf{g}'} \cdot \mathbf{A}_{\mathrm{L}})] Q^{\mathrm{III}}_{\mathbf{g}i;\mathbf{g}'i'},$$

$$S^{--}_{\mathbf{g}i;\mathbf{g}'i'} = \exp[-i(\mathbf{K}^-_{\mathbf{g}} \cdot \mathbf{A}_{\mathrm{L}} - \mathbf{K}^-_{\mathbf{g}'} \cdot \mathbf{A}_{\mathrm{R}})] Q^{\mathrm{IV}}_{\mathbf{g}i;\mathbf{g}'i'} \quad (40)$$

for the given ω and $\mathbf{k}_{\parallel}$. The phase factors in Eq. (40) arise from the need to refer all waves to a common origin.

Alternatively, one can calculate the complex frequency band structure of the EM field in an infinite photonic crystal, using the Q matrices of the unit slice, in the manner described in Ref. 2.

We consider a simple cubic (sc) crystal, with lattice constant $a=6.5c/\omega_p$, of nonabsorbing metallic spheroids ($A=2.065c/\omega_p$, $B=1.877c/\omega_p$), in air, and view the crystal as a sequence of (001) planes of particles. In the left panel of Fig. 6 we show the photonic band structure of this crystal along the [001] direction ($\mathbf{k}_{\parallel}=\mathbf{0}$), together with the corresponding results for the same system with the spheroids being replaced by spheres of equal volume ($S=c/\omega_p$). The symmetry of the bands along this direction, for both crystals, is that of the C_{4v} group: Δ_1, Δ_2, $\Delta_{1'}$, $\Delta_{2'}$, and Δ_5.[37] The bands Δ_1, Δ_2, $\Delta_{1'}$, and $\Delta_{2'}$ are nondegenerate, and Δ_5 is doubly degenerate. We note that the (001) surface of the crystals under consideration is a plane of mirror symmetry and, therefore, the frequency bands appear in pairs: $k_z(\omega, \mathbf{k}_{\parallel})$ and $-k_z(\omega, \mathbf{k}_{\parallel})$; for this reason, in Fig. 6, we show the bands only for positive k_z.

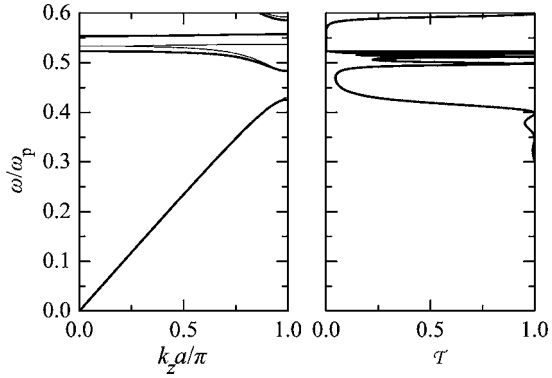

FIG. 6. Left panel: The photonic band structure of a sc photonic crystal, with lattice constant $a=6.5c/\omega_p$, of nonabsorbing metallic particles (thick lines, oblate spheroids, with $A=2.065c/\omega_p$ and $B=1.877c/\omega_p$; thin lines, spheres with $S=c/\omega_p$), in air, along the [001] direction. Right panel: Transmittance at normal incidence of a slab of eight (001) planes of the above crystal of spheroids.

In the long-wavelength limit we obtain a linear dispersion curve, of Δ_5 symmetry, as expected for propagation in a homogeneous effective medium with a frequency-independent dielectric constant $\bar{\epsilon}=\lim_{\omega\to 0}\{[\epsilon_s(1+2f)+2(1-f)]/[\epsilon_s(1-f)+(2+f)]\}=1.05$, which is the same for both crystals. This extended effective-medium band is folded within the first Brillouin zone and a Bragg gap opens up at the Brillouin zone boundaries. In each case, within the gap, there are two relatively flat bands, a lower band of Δ_5 and a higher one of Δ_1 symmetry, which originate from the dipole surface-plasmon modes of the metallic particles: these bands are formed from the corresponding modes of the individual (001) planes of particles, weakly interacting between them. In the case of the crystal of spheres, the two flatbands are close to each other and converge at the center of the Brillouin zone to a threefold degenerate point of Γ_{15} symmetry, while in the crystal of spheroids the two flatbands are well separated from each other. This important difference between the two crystals may be useful in the design of (polarization-selective) filters and single-mode coupled-resonator optical waveguides[38,39] based on photonic crystals of nonspherical particles. According to the discussion in the previous section, the nondegenerate bands along the [001] direction of these crystals cannot be excited by an externally incident wave because they do not have the proper symmetry. However, these bands survive for $\mathbf{k}_{\parallel} \neq \mathbf{0}$, where they couple with an incident wave of the same $\mathbf{k}_{\parallel}$ leading to measurable transmit-

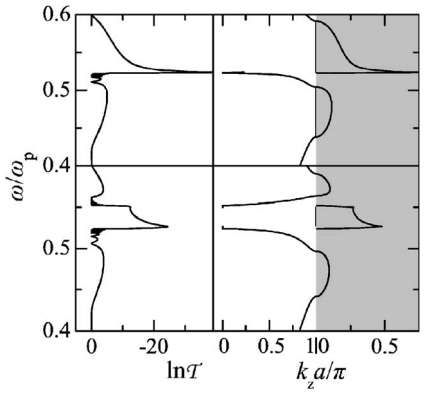

FIG. 7. Left panel: Transmission coefficient of an *s*- (upper diagram) and a *p*- (lower diagram) polarized wave incident on a slab of eight (001) planes of the photonic crystal of spheroids under consideration with $\mathbf{k}_\parallel=(0.3\pi/a,0)$. Right panel: The corresponding complex band structure for the Q_2 (upper diagram) and the Q_1 (lower diagram) bands. In the gap regions we show the eigenvalues k_z with the smallest imaginary part (plotted in the shaded area) which may belong to different bands over different regions of frequency.

tance (see Fig. 7 below). In the right panel of Fig. 6 we show the transmittance of a slab of the crystal of spheroids consisting of eight (001) planes. The transmittance opposite the extended band is about unity and exhibits the well-known Fabry-Pérot oscillations due to multiple scattering between the surfaces of the slab; the period of these oscillations corresponds to $k_z a/\pi=1/8$, as expected for the given slab thickness. In the gap regions and also within the region of the Δ_1 band the transmission coefficient practically vanishes.

In the right panel of Fig. 7 we show the photonic band structure of the crystal of spheroids in more detail, over a limited frequency region about the dipole surface-plasmon resonances, for $\mathbf{k}_\parallel=(0.3\pi/a,0)$. Apart from the ordinary frequency bands (k_z is real) we show, over the gap regions, the real-frequency lines with the smallest imaginary part of k_z. For $\mathbf{k}_\parallel=(k_x,0)$, $0<k_x<\pi/a$, the point group of the wave vector is the C_{1h} group, and, according to group theory, we obtain from the Δ_1 band (for $\mathbf{k}_\parallel=\mathbf{0}$) one Q_1 band and from the Δ_5 band one Q_1 and one Q_2 band, as shown in the right panel of Fig. 7. A *s*- or *p*-polarized EM wave incident on a finite (001) slab of the crystal with $\mathbf{k}_\parallel=(k_x,0)$ excites bands of Q_2 or Q_1 symmetry, respectively, and through them is transmitted to the other side of the slab. In the regions of frequency gaps there are no propagating Bloch modes, and there the transmission coefficient is determined from the complex band of the proper symmetry which has the smallest imaginary part: the wave decreases exponentially within the slab with an attenuation coefficient equal to Im $k_z(\omega)$ of this band, as shown in the left panel of Fig. 7.

V. CONCLUSIONS

In summary, we presented an extension of the LMSM to photonic crystals consisting of nonspherical particles in a homogeneous host medium. We incorporated the EBCM into the LMSM formalism and showed that the method retains its efficiency and accuracy, at least in cases where the shape of the particles does not deviate strongly from the sphere. We demonstrated the applicability of the method on a specific example of a photonic crystal of metallic oblate spheroids. We analyzed transmission and absorption spectra of finite slabs of this crystal by reference to relevant complex-band-structure and density-of-states diagrams, and showed that nonspherical particles provide an additional degree of freedom for tailoring the characteristics of localized resonant modes of photonic crystals. This may be useful in a variety of applications, e.g., the design of light absorbers, filters, and single-mode waveguides.

ACKNOWLEDGMENTS

This work was supported by the Empeirikeion Foundation and by the research program "Kapodistrias" of the University of Athens. G.G. is supported by the State Scholarships Foundation (I.K.Y.), Greece.

[1] N. Stefanou, V. Karathanos, and A. Modinos, J. Phys.: Condens. Matter **4**, 7389 (1992).
[2] N. Stefanou, V. Yannopapas, and A. Modinos, Comput. Phys. Commun. **113**, 49 (1998).
[3] N. Stefanou, V. Yannopapas, and A. Modinos, Comput. Phys. Commun. **132**, 189 (2000).
[4] K. Ohtaka and Y. Tanabe, J. Phys. Soc. Jpn. **65**, 2265 (1996).
[5] K. Ohtaka and Y. Tanabe, J. Phys. Soc. Jpn. **65**, 2276 (1996).
[6] K. Ohtaka and Y. Tanabe, J. Phys. Soc. Jpn. **65**, 2670 (1996).
[7] V. Yannopapas, A. Modinos, and N. Stefanou, Phys. Rev. B **60**, 5359 (1999).
[8] A. Modinos, N. Stefanou, and V. Yannopapas, Opt. Express **8**, 197 (2001).
[9] N. Stefanou, A. Modinos, and V. Yannopapas, Solid State Commun. **118**, 69 (2001).
[10] A. Moroz, Phys. Rev. B **66**, 115109 (2002).
[11] T. V. Teperik, V. V. Popov, and F. J. García de Abajo, Phys. Rev. B **71**, 085408 (2005).
[12] F. J. García de Abajo, G. Gómez-Santos, L. A. Blanco, A. G. Borisov, and S. V. Shabanov, Phys. Rev. Lett. **95**, 067403 (2005).
[13] M. H. Kok, R. Ma, J. C. W. Lee, W. Y. Tam, C. T. Chan, P. Sheng, and K. W. Cheah, Phys. Rev. E **72**, 047601 (2005).
[14] V. Yannopapas and A. Moroz, J. Phys.: Condens. Matter **17**, 3717 (2005).
[15] G. Gantzounis and N. Stefanou, Phys. Rev. B **72**, 075107 (2005).
[16] V. Yannopapas, N. Stefanou, and A. Modinos, Phys. Rev. Lett. **86**, 4811 (2001).
[17] Z. L. Wang, C. T. Chan, W. Y. Zhang, Z. Chen, N. B. Ming, and P. Sheng, Phys. Rev. E **67**, 016612 (2003).
[18] V. Yannopapas, A. Modinos, and N. Stefanou, Phys. Rev. B **68**, 193205 (2003).

[19] V. Yannopapas and N. Stefanou, Phys. Rev. B **69**, 012408 (2004).
[20] Y. Kurokawa, H. Miyazaki, and Y. Jimba, Phys. Rev. B **69**, 155117 (2004).
[21] G. Gantzounis, N. Stefanou, and V. Yannopapas, J. Phys.: Condens. Matter **17**, 1791 (2005).
[22] Y. Kurokawa, H. Miyazaki, H. T. Miyazaki, and Y. Jimba, J. Phys. Soc. Jpn. **74**, 924 (2005).
[23] K. Ohtaka and M. Inoue, Phys. Rev. B **25**, 677 (1982).
[24] V. Yannopapas, A. Modinos, and N. Stefanou, Phys. Rev. B **65**, 235201 (2002).
[25] R. Sainidou, N. Stefanou, and A. Modinos, Phys. Rev. B **69**, 064301 (2004).
[26] K. Ohtaka, J. Inoue, and S. Yamaguti, Phys. Rev. B **70**, 035109 (2004).
[27] W. Y. Zhang, X. Y. Lei, Z. L. Wang, D. G. Zheng, W. Y. Tam, C. T. Chan, and P. Sheng, Phys. Rev. Lett. **84**, 2853 (2000).
[28] Y. A. Vlasov, X. Z. Bo, J. C. Sturm, and D. J. Norris, Nature (London) **414**, 289 (2001).
[29] N. Pinna, M. Maillard, A. Courty, V. Russier, and M. P. Pileni, Phys. Rev. B **66**, 045415 (2002).
[30] F. Lopez-Tejeira, T. Ochiai, K. Sakoda, and J. Sanchez-Dehesa, Phys. Rev. B **65**, 195110 (2002).
[31] R. Fenollosa and F. Meseguer, Adv. Mater. (Weinheim, Ger.) **15**, 1282 (2003).
[32] V. Yannopapas, A. Modinos, and N. Stefanou, Opt. Quantum Electron. **34**, 227 (2002).
[33] K. P. Velikov, A. Moroz, and A. van Blaaderen, Appl. Phys. Lett. **80**, 49 (2002).
[34] M. I. Mishchenko, L. D. Travis, and A. A. Lacis, *Scattering, Absorption, and Emission of Light by Small Particles* (Cambridge University Press, Cambridge, U.K., 2002).
[35] A. Moroz, Appl. Opt. **44**, 17 (2005).
[36] N. W. Ashcroft and N. D. Mermin, *Solid State Physics* (Saunders, New York, 1976).
[37] J. F. Cornwell, *Group Theory and Electronic Energy Bands in Solids* (North-Holland, Amsterdam, 1969).
[38] N. Stefanou and A. Modinos, Phys. Rev. B **57**, 12127 (1998).
[39] A. Yariv, Y. Xu, R. K. Lee, and A. Scherer, Opt. Lett. **24**, 711 (1999).